RSC Advances

PAPER

View Article Online
View Journal | View Issue

Cite this: *RSC Adv.*, 2023, **13**, 8822

Metalloporphyrin modified defective TiO_2 porous cages with the enhanced photocatalytic activity for coupling of hydrogen generation and tetracycline removal†

Haiyue Lu,[a] Xiaohua Wang,[a] Gen Li,[a] Baicheng Liao,[a] Zhizhi Gu,[c] Xiuli Zhang,*[a] Feifei Yuan,[ab] Jing Tong[a] and Liyong Chen *[ab]

Integration of molecular transition-metal complexes and semiconductors is an appealing method to develop high-performance hybrid photocatalysts based on improvement of their solar energy harvesting ability and photogenerated charge carrier separation efficiency. Herein, Cu-TCPP modified TiO_2 porous cages with oxygen vacancy defects, derived from NH_2-MIL-125(Ti) nanocrystals, are successfully prepared to form PC-TiO_2-*d*/Cu-TCPP hybrids *via* a surface assembly process. The PC-TiO_2-*d*/Cu-TCPP hybrid shows an enhanced photodegradation efficiency (73.7%, 95.4%) towards tetracycline in the air under visible light or the simulated sunlight irradiation compared to PC-TiO_2-*d* (33.7%, 81.1%) within 100 min. Moreover, the photocatalytic system is applicable to coupling both processes of solar fuel production and pollutant degradation. The PC-TiO_2-*d*/Cu-TCPP hybrid exhibits a high hydrogen evolution rate of ~2 mmol g^{-1} h^{-1} in the aqueous solution of tetracycline in an inert atmosphere upon irradiation by the simulated sunlight. In contrast, an inferior photocatalytic performance of hydrogen evolution is observed in pure water without the addition of tetracycline. Finally, the high sustainability of PC-TiO_2-*d*/Cu-TCPP is mainly attributed to the strong interaction between the molecular photosensitizer and the semiconductor photocatalyst by oxygen vacancies and Cu(II) ions.

Received 6th January 2023
Accepted 9th March 2023

DOI: 10.1039/d3ra00105a

rsc.li/rsc-advances

Introduction

With the wide use of drug molecules to ward off various diseases, pharmaceutical contaminants have gradually received tremendous attention due to being detected in diverse aquatic environments and sediment worldwide.[1–4] Among these contaminants, antibiotics such as tetracycline are extensively and increasingly used in human and veterinary medicine, and thus becoming a significant class of emerging pharmaceutical contaminants.[5–12] Photodegradation is generally the most effective and economical method for the removal of organic pollutants from the environment.[13–16] Generally, in the redox process, organic pollutants are oxidized into CO_2, H_2O and other fragments by accepting holes from photocatalysts or donating electrons to hydroxyl radicals; oxygen molecules that receive electrons from photocatalysts are reduced into superoxide radicals that are able to react with water molecules to produce hydroxyl radicals.[17–19] However, instead of the traditional redox process, if the half-reaction of oxygen reduction is replaced by solar-to-fuel conversion, it is possible to achieve the simultaneous occurrence of solar fuel synthesis and organic pollutant degradation in the same photocatalytic system.[20,21] Therefore, by using the contaminated water from tetracycline as feedstock, the mitigation of the pharmaceutical pollutant together with the generation of hydrogen as a green fuel may be achieved. In contrast to kinetically sluggish water oxidation half reaction leading to easy recombination of the photo-generated electron–hole pair, tetracycline as sacrificial electron donors enable rapid consumption of holes, benefiting for high-efficiency photocatalytic hydrogen generation.

The low-cost and steady titanium dioxide (TiO_2) as a sophisticated photocatalyst has been studied for the integrated reactions of H_2 evolution coupled with degradation of organic pollutants.[22,23] However, the photo response in the ultraviolet region caused by the wide band gap has negatively affected the widespread applications of TiO_2 in photocatalysis.[24] For this reason, many reports have focused on the improvement of the photocatalytic activity of TiO_2 by extending the wavelength range of light absorption.[25] Combination of TiO_2 with molecular

[a]*Department of Pharmaceutical Engineering, Bengbu Medical College, Bengbu, 233030, China. E-mail: lychen@bbmc.edu.cn*

[b]*Anhui Province Key Laboratory of Translational Cancer Research, Bengbu Medical College, Bengbu, 233030, China*

[c]*College of Fisheries and Life Science, Dalian Ocean University, Dalian, 116023, China*

† Electronic supplementary information (ESI) available: XRD patterns, SEM images, TEM images, XPS spectra, Raman spectra, N_2 sorption isotherms, UV-visible absorption spectra and photo-degradation of tetracycline. See DOI: https://doi.org/10.1039/d3ra00105a

sensitizers is considered as one of the effective methods to pursue the purpose. Introducing molecular catalysts/co-catalysts to solid supports to form heterogeneous catalysts has recently attracted great interest.[26–28] The behaviour can bring some additional advantages, including high-efficiency charge carrier separation between molecules and supports and long-term sustainability of molecules. Porphyrin is an important class of dyes with a wide absorption spectrum and a high extinction coefficient; and the easy modification of porphyrin, such as introducing different functional groups on the *meso*-positions or β-sites and coordination of metal ions with nitrogen atoms, facilitates the well loading of porphyrin molecules into the surfaces of substrates.[29–31] Herein, this research aims to develop an efficient synthetic method for preparation of a hybrid photocatalyst consisting of metalloporphyrin-loaded TiO_2 and explore its effectiveness in degrading tetracycline and producing hydrogen under visible light irradiation in an aqueous solution of tetracycline.

Results and discussion

Synthesis of PC-TiO_2-*d*/Cu-TCPP hybrids

TiO_2 with oxygen vacancy defects (TiO_2-*d*), which has been extensively investigated in the field of catalysis,[32–36] can easily anchor guest species to construct stable multi-component materials, and porous hollow structures allow to provide much more sites for catalysis and improve mass transfer.[37] Typical TiO_2-*d* porous cages (PC-TiO_2-*d*) are produced by a two-step synthetic procedure.[38,39] An amino acid-assisted solvothermal route to accomplish the NH_2-MIL-125(Ti) transformation in solution was used to prepare nanosheets assembled porous cages of titanium oxides (Fig. S1†), and the as-formed precursor was subsequently calcinated in air to form PC-TiO_2-*d* (Fig. S2†). The anatase PC-TiO_2-*d* corresponding to the tetragonal crystal structure was confirmed by the X-ray diffraction (XRD) pattern (Fig. S2a†). The X-ray photoelectron spectroscopy (XPS) of PC-TiO_2-*d* provided the surface elemental analysis of O and Ti, whose molar ratio is less than 2 : 1, suggesting the possible presence of oxygen vacancies. The O 1s XPS spectrum clearly shows two peaks with the binding energy of 529.9 and 531.7 eV, corresponding to lattice oxygen and oxygen vacancy, respectively; the negative shift of Ti(iv) core-level binding energy of Ti 2p3/2 and Ti 2p1/2 can be found in Ti 2p XPS spectrum at 458.65 and 464.4 eV (Fig. S3†).[40,41] These results further unveil the presence of oxygen vacancies. PC-TiO_2-*d* was characterized by scanning electron microscopy (SEM) and transmission electron microscopy (TEM) images, in which TiO_2-*d* nanoparticles with 20–30 nm in diameters assembled into cages were found (Fig. S2b and c†). In addition, the Brunauer–Emmett–Teller (BET) N_2 sorption isotherm of PC-TiO_2-*d* was measured at 77 K to reveal the porous structures. A type-IV hysteresis loop at relative pressure P/P_0 higher than 0.4 were observed from the sorption isotherm, signifying the presence of mesoporous structures (Fig. S4a†).

The Cu-TCPP (TCPP: tetrakis(4-carboxyphenyl)porphyrin) complex was prepared by a typical synthetic procedure, where $CuCl_2$ and tetrakis(4-methoxycarbonylphenyl)porphyrin (TCPP-OMe) was firstly refluxed and subsequently treated by HCl.[42] The as-made Cu-TCPP that was confirmed by mass spectrum (Fig. S5†) was mixed with PC-TiO_2-*d* in dimethyl formamide (DMF) to prepare the composite of Cu-TCPP loaded TiO_2-*d* (PC-TiO_2-*d*/Cu-TCPP). The porous cages were still observed in SEM and TEM images of the composite, and anatase PC-TiO_2-*d* was not changed according to its XRD pattern after loading of Cu-TCPP (Fig. 1a, b, and d). Elemental mapping images of Ti and Cu show that both elements are homogeneously dispersed in whole porous cages (Fig. 1c). The Ti 2p core electron binding energy of PC-TiO_2-*d*/Cu-TCPP is slightly different from that of PC-TiO_2-*d*, signifying the difference in chemical environments of Ti(iv) species between PC-TiO_2-*d*/Cu-TCPP and PC-TiO_2-*d* (Fig. 2a). In the deconvoluted O 1s XPS spectrum, a new peak with a binding energy of 530.2 eV is observed, possibly corresponding to the O 1s signal from C–O (Fig. 2b). The peak at 530.2 eV cannot be clearly discernible in the overall O 1s XPS spectrum because of the overlapping of both peaks of C–O and lattice oxygen. More important, both signals of Cu 2p and N 1s were still detected in the survey XPS spectrum of PC-TiO_2-*d*/Cu-TCPP (Fig. 2c and d). The high-resolution Cu 2p XPS spectrum was deconvoluted into four peaks based on the Shirley type background subtraction method (Fig. 2c). Except for two satellite peaks, others are main peaks of 2p(3/2) and 2p(1/2) of Cu(II). In the N 1s XPS spectrum (Fig. 2d), the redistribution of electron density between pyrro-N and aza-N after introducing of Cu(II) into the centre of TCPP leads to shifting of two signals to 400.7 and 398.55 eV and an increase of the signal with the low binding energy corresponding to aza-N in intensity.[43,44] These experimental observations reveal that Cu-TCPP is successfully anchored on the surfaces of PC-TiO_2-*d* (Fig. 2c). In addition, Raman spectra of PC-TiO_2-*d*/Cu-TCPP and Cu-TCPP show the similar characteristic peaks between 800 and 2000 cm^{-1}, assigned to C–N, C–C, and phenyl of porphyrin rings, further confirming the formation of PC-TiO_2-*d*/Cu-TCPP composites (Fig. S6†).[43]

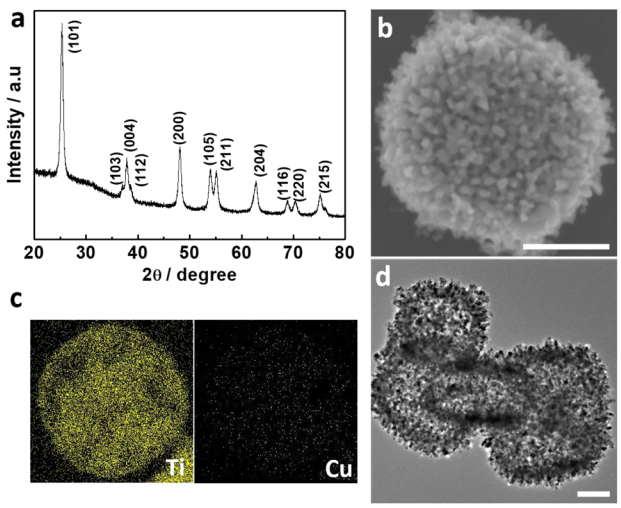

Fig. 1 PC-TiO_2-*d*/Cu-TCPP porous cages: (a) XRD pattern, (b) SEM image, (c) energy dispersive X-ray spectroscopy elemental mapping images of Ti and Cu and (d) TEM image. All scale bars are 200 nm.

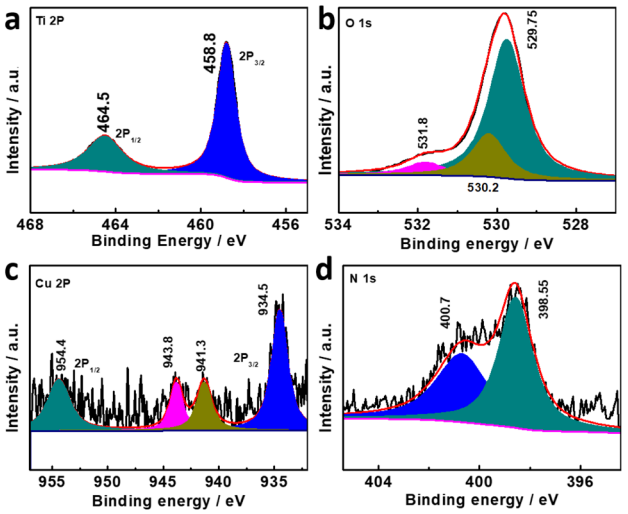

Fig. 2 High-resolution XPS spectra of (a) Ti 2p, (b) O 1s, (c) Cu 2p and (d) N 1s in PC-TiO_2-*d*/Cu-TCPP porous cages.

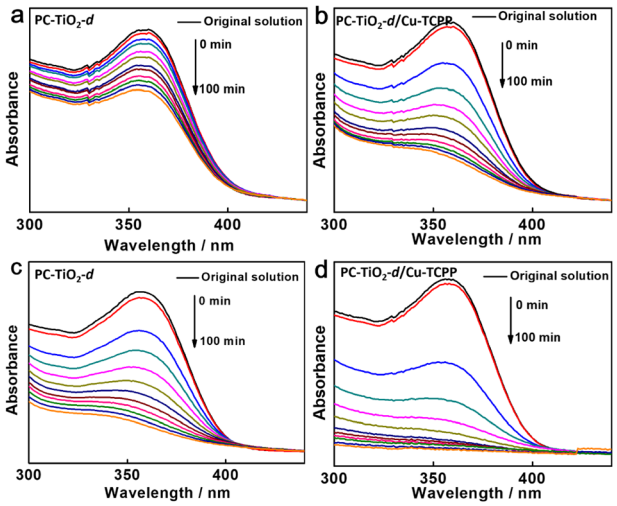

Fig. 3 UV-visible absorption spectra of tetracycline aqueous solution in the presence of (a and c) PC-TiO_2-*d*, and (b, d) PC-TiO_2-*d*/Cu-TCPP after irradiation by visible light (upper) or simulated sunlight (lower) with different times.

Porphyrins generally are chromophores in the visible region with strong absorption ability, including Soret band absorption at short wavelength and Q-band absorption at long wavelength region, which can be found in Cu-TCPP absorption spectrum (Fig. S7a†). In the UV-vis absorption spectrum of PC-TiO_2-*d*/Cu-TCPP, the absorbance in the visible region is greatly increased in comparison with PC-TiO_2-*d*, and two distinct absorption peaks assigned as Soret band and Q-band of Cu-TCPP can be found (Fig. S7b†).[45] On the basis, the PC-TiO_2-*d*/Cu-TCPP hybrid could possess high-efficient photocatalytic activity upon visible light irradiation.

Photocatalytic performance of PC-TiO_2-*d*/Cu-TCPP hybrids

To study the photocatalytic performance of PC-TiO_2-*d*/Cu-TCPP towards tetracycline degradation, PC-TiO_2-*d*/Cu-TCPP powder (5 mg) was dispersed into the dilute aqueous solution of tetracycline (4.5×10^{-5} M, 60 mL). Prior to light irradiation, the resulting mixture was gently stirred in darkness for 30 min to fully absorb tetracycline into PC-TiO_2-*d*/Cu-TCPP. Afterwards, the photo-degradation experiment was performed under irradiation of a 300 W Xe short arc lamp equipped with a 420 nm cut-off filter. According to the change of absorbance of the characteristic absorption peak at 358 nm in the UV-vis absorption spectrum of tetracycline, tetracycline was gradually degraded under visible light irradiation (Fig. 3). While the irradiation time is prolonged to 100 min, the degradation percentage (*P*%) of tetracycline is about 73.7% (Fig. 3b) after subtraction of tetracycline adsorption. In contrast, PC-TiO_2-*d* shows low degradation percentage (33.4%) under otherwise identical conditions (Fig. 3a). This should be attributed to weak light absorption ability of PC-TiO_2-*d* in the visible region. Predictably, if the simulated sunlight by using an AM 1.5G filter to replace the 420 nm cut-off filter was employed as light source, both PC-TiO_2-*d*/Cu-TCPP and PC-TiO_2-*d* exhibit the enhanced photo-degradation performance of tetracycline (*P*%: 95.4% and 81.1%, Fig. 3e and d) after subtraction of tetracycline adsorption. Hence, in the photo-degradation process, we speculate that PC-TiO_2-*d* could serve as photocatalysts and Cu-TCPP could function as photosensitizers to mediate the electron transfer between photocatalysts and electron donors. It is further confirmed by two parallel experiments, wherein the degradation percentage of tetracycline is decreased to 11.7% and 4%, respectively, under simulated sunlight irradiation, if Cu-TCPP was used alone or any catalysts were not added to the photo-degradation system (Fig. S8†).

The recyclability of PC-TiO_2-*d*/Cu-TCPP was also studied under visible light/simulated sunlight irradiation. The obvious loss of the photo-degradation performance towards tetracycline did not arise after six successive recycling runs of PC-TiO_2-*d*/Cu-TCPP (Fig. S9†). XRD pattern and SEM and TEM images of PC-TiO_2-*d*/Cu-TCPP up to the sixth run reveal the high stability of the structure and morphology of PC-TiO_2-*d* (Fig. S10a–c†). The stable photocatalytic performance of PC-TiO_2-*d*/Cu-TCPP is also related to the strong interaction between Cu-TCPP and PC-TiO_2-*d*. The detachment of Cu-TCPP from PC-TiO_2-*d* surfaces seldom occurs during the photo-degradation process. The characteristic absorption peaks of Cu-TCPP can be found in the UV-vis absorption spectrum of PC-TiO_2-*d*/Cu-TCPP after being used six times (Fig. S10d†), revealing the presence of Cu-TCPP. The photocatalytic system including Cu-TCPP and PC-TiO_2-*d* shows low photocatalytic activity (~49%) towards tetracycline degradation under visible light irradiation. The experimental observation further provides the evidence for the assessment of the stable PC-TiO_2-*d*/Cu-TCPP hybrids. In contrast, TCPP modified PC-TiO_2-*d* (PC–TiO_2-*d*/TCPP) shows poor recyclability under visible light irradiation, and its photocatalytic activity is similar to that of PC-TiO_2-*d* after three recycling runs (Fig. S11†). The characteristic absorption peaks of TCPP almost cannot be found in the UV-vis absorption spectrum of PC-TiO_2-*d*/TCPP used (Fig. S12†). Hence, Cu(II) ions could play an essential role in anchoring Cu-TCPP molecules on the surfaces of PC-TiO_2-*d* by coordination interaction.

The loading amount of Cu-TCPP could also affect the photocatalytic activity of PC-TiO_2-*d*/Cu-TCPP towards tetracycline degradation (Fig. S13†). If decreasing the loading amount of Cu-TCPP from 5 : 100 to 1 : 100, the degradation percentage of tetracycline is declined to 68.6% upon visible light irradiation. The possible explanation is that a small amount of Cu-TCPP cannot provide enough photo-generated electrons to sensitize the photocatalyst PC-TiO_2-*d*. If increasing the loading amount of Cu-TCPP to 10 : 100 and 20 : 100, the degradation percentage of tetracycline is reduced to 62.7% and 53.3%, respectively. The possible scenario is that much more catalytic sites of PC-TiO_2-*d* was shielded by Cu-TCPP. If the loading amount of Cu-TCPP continued to increase, the photocatalytic activity of PC-TiO_2-*d*/Cu-TCPP did not decrease significantly and the degradation percentage of tetracycline was kept at ~50%. The experimental result may be attributed to the saturated adsorption of Cu-TCPP on the surfaces of PC-TiO_2-*d*.

Porous hollow structures can also be helpful for the enhancement of photocatalytic performance towards tetracycline degradation. For this purpose, TiO_2 nanoparticles (TiO_2-*n*) were successfully prepared by direct thermal treatment of NH_2-MIL-125(Ti) at air atmosphere (Fig. S14†). The as-made TiO_2-*n* displays the low photo-degradation percentage of tetracycline (19.6%) while irradiation of visible light (Fig. S15a†). After loading Cu-TCPP, TiO_2-*n* shows enhanced photocatalytic activity (*P*%: 38%) (Fig. S15b†). Nonetheless, whatever TiO_2-*n* or TiO_2-*n* loaded with Cu-TCPP possesses inferior photocatalytic activity in terms of PC-TiO_2-*d* or PC-TiO_2-*d*/Cu-TCPP. These results confirm that porous cage morphologies make the significant contribution to the photocatalytic performance of tetracycline degradation possibly due to large surface area with much more catalytic sites and easier transport for guest species.

Previously, a pioneer research work involved in the coupling of fuel preparation and pollution utilisation *via* a photocatalytic process.[20] On this basis, PC-TiO_2-*d*/Cu-TCPP was used to study the photocatalytic performance for hydrogen evolution and tetracycline degradation in the aqueous solution of tetracycline under simulated sunlight irradiation in Ar atmosphere. While irradiation time is prolonged to 4 h, the hydrogen evolution rate is ~2.3 mmol g^{-1} h^{-1} and simultaneously tetracycline degradation is ~73.8% (Fig. 4). The quantum yield (QY) is about 0.22% at 475 nm (100 mW cm^{-2}). In our case, if the photocatalytic system was not inclusive of tetracycline, the hydrogen evolution is difficultly found under the same conditions. In addition, the aqueous solution of tetracycline without PC-TiO_2-*d*/Cu-TCPP cannot generate hydrogen and degrade tetracycline as well upon simulated sunlight irradiation in Ar atmosphere. Hence, PC-TiO_2-*d*/Cu-TCPP serves as photocatalysts that facilitate the coupling of the hydrogen evolution and tetracycline degradation. PC-TiO_2-*d*/Cu-TCPP exhibits high stability in the coupling process of hydrogen evolution and tetracycline degradation, and the hydrogen evolution rate is still as high as ~2 mmol g^{-1} h^{-1} after six successive recycling runs. If PC-TiO_2-*d* instead of PC-TiO_2-*d*/Cu-TCPP was added to the photocatalytic system, the hydrogen evolution rate was decreased to ~114 μmol g^{-1} h^{-1} within 4 h.

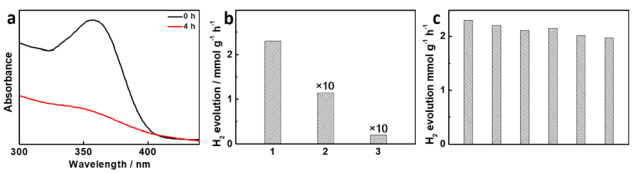

Fig. 4 (a) UV-visible absorption spectra of tetracycline aqueous solution upon irradiation of simulated sunlight for 4 h in the presence of PC-TiO_2-*d*/Cu-TCPP in Ar atmosphere, (b) photocatalytic hydrogen evolution performance of (1) PC-TiO_2-*d*/Cu-TCPP and (2) PC-TiO_2-*d* in tetracycline aqueous solution and (3) PC-TiO_2-*d*/Cu-TCPP in pure water, and (c) the recyclability of PC-TiO_2-*d*/Cu-TCPP in the coupling reaction between hydrogen evolution and tetracycline degradation.

The enhanced photocatalytic mechanism

Except for large specific surface areas and porous structures of PC-TiO_2-*d* and the strong light absorption ability of Cu-TCPP in the visible region, the enhanced photocatalytic activity of PC-TiO_2-*d*/Cu-TCPP is greatly dependent on the density of photo-generated electrons and the charge transfer efficiency at the interfaces of photocatalysts and substrates. The PC-TiO_2-*d*/Cu-TCPP hybrids exhibit the significant enhancement of photocurrent density at 1.0 V *vs.* Ag/AgCl in terms of pure PC-TiO_2-*d* under chopped simulated sunlight illumination (Fig. 5a), signifying that after loading Cu-TCPP, PC-TiO_2-*d* shows higher efficiency in separation of photo-generated charges. Electrochemical impedance spectroscopy (EIS) was used to identify charge transfer resistance related to Faraday reactions based on diameters of Nyquist plots in the high frequency region (Fig. 5b). The Nyquist plot of PC-TiO_2-*d*/Cu-TCPP shows a smaller diameter than that of PC-TiO_2-*d*, and thus PC-TiO_2-*d*/Cu-TCPP had higher charge transfer efficiency at the interfaces between electrodes and electrolytes. These experimental observations further suggest that PC-TiO_2-*d*/Cu-TCPP possesses the superior photo-degradation performance in terms of PC-TiO_2-*d* without loading of Cu-TCPP.

The high-efficient interfacial electron transfer between Cu-TCPP and PC-TiO_2-*d* is mainly determined by their energy

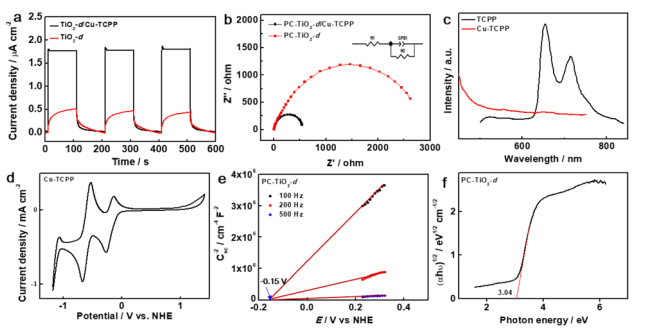

Fig. 5 (a) Photocurrent transient responses at 1.0 V *vs.* Ag/AgCl upon simulated sunlight chopped irradiation and (b) Nyquist plots at 1.0 V *vs.* Ag/AgCl of PC-TiO_2-*d*/Cu-TCPP and PC-TiO_2-*d* (inset: equivalent circuit). (c) Photoluminescence spectra of Cu-TCPP and TCPP. (d) Cyclic voltammogram of Cu-TCPP. (e) M–S plots collected at different frequencies. (f) Tauc plot of PC-TiO_2-*d*.

levels. The electrons of TCPP can transfer to metal centre Cu after excitation, which was confirmed by photoluminescence quench of Cu-TCPP (Fig. 5c). The cyclic voltammetry (CV) curve of Cu-TCPP shows two pairs of anodic and cathodic peaks, revealing that Cu-TCPP undergoes two reversible one-electron reduction steps at half-wave potential $E_{1/2}$ of ~−0.2 and −0.6 V (*vs.* NHE), assigned to the reduction of the metal centre, that is, Cu(II) to Cu(I) and Cu(I) to Cu(0), respectively (Fig. 5d).[46] The energy position of the conduction band of PC-TiO_2-*d* was estimated to be ~−4.25 eV that is located at more negative values (~−0.1 V) of the energy position of its flat band determined by Mott–Schottky (M–S) curves at different applied potentials (Fig. 5e).[47,48] The experimental value of the conduction band is very close to the calculated value according to the empirical equation: $E_c = \chi + E_0 - 0.5E_g$, wherein χ is the absolute electronegativity of PC-TiO_2-*d*, E_0 is normal hydrogen electrode redox level *versus* the absolute vacuum scale, and E_g is the band gap of PC-TiO_2-*d*.[49] Hence, the excited electrons of Cu-TCPP can inject into the conduction band of PC-TiO_2-*d* from Cu centres based on their energy levels.

In accordance with the aforementioned experimental data, the enhanced photocatalytic mechanism for tetracycline degradation could involve in the sensitization process of Cu-TCPP to PC-TiO_2-*d*. In detail, upon light irradiation, the photogenerated electrons in Cu-TCPP are trapped by Cu(II) centres, producing Cu(I) and Cu(0) species by the ligand-to-metal charge transfer process, and the recombination of electron–hole pairs in Cu-TCPP is suppressed. Subsequently, the most photogenerated electrons are injected into the conduction band of PC-TiO_2-*d* from Cu species (Fig. 6, left), further facilitating the separation of charge carriers. According to energy levels between the conduction band of PC-TiO_2-*d* and the redox potential of $O_2/O_2^{\bullet}$, the excited electrons can be transferred to O_2 to form superoxide radicals ($O_2^{\bullet-}$) (Fig. 6, left).[18] In addition, the valence band of PC-TiO_2-*d* is about −7.29 eV in accordance with its conduction band of its band gap that is obtained from Tauc plot (Fig. 5f). Hence, the holes located at the valence band of PC-TiO_2-*d* can oxidize H_2O to produce hydroxyl radicals ($OH^{\bullet}$) (Fig. 6, left).[18] The holes in the HOMO of TCPP, however, are unfavourable for the generation of $OH^{\bullet}$ due to high energy level of HOMO (−5.58 eV), and possibly oxidize tetracycline to suppress TCPP degradation.[50] To clear the role of the active species of holes, $O_2^{\bullet-}$ and $OH^{\bullet}$ in the tetracycline degradation process, some parallel experiments were carried out. While ethylenediaminetetraacetic acid (EDTA) and *tert*-butanol (TBA) that function as effective hole and $OH^{\bullet}$ scavengers, respectively, were added to the photocatalytic system,[51] the degradation percentage of tetracycline in both experiments was decreased. Moreover, replacing O_2 with Ar in the reaction atmosphere results in a decrease in the photo-degradation efficiency of tetracycline. As a result, these active species of holes, $O_2^{\bullet-}$ and $OH^{\bullet}$ exerted considerable influence on the photocatalytic activity of PC-TiO_2-*d*/Cu-TCPP in the tetracycline degradation process (Fig. 6, right). On the basis, the coupling reactions of H_2 evolution and tetracycline removal in Ar atmosphere can be achieved because holes and $OH^{\bullet}$ radicals enable tetracycline degradation to occur, and the excited electrons located at the conduction band of PC-TiO_2-*d* can transfer directly to H^+ ions to form H_2 without interference from oxygen (Fig. 6, left and right).

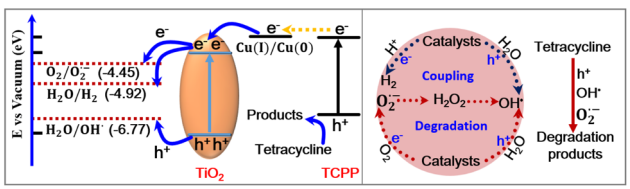

Fig. 6 Energy positions of corresponding redox couples and catalysts (left) and schematic illustrating the photocatalytic mechanism of PC-TiO_2-*d*/Cu-TCPP towards tetracycline degradation or coupling of hydrogen evolution and tetracycline degradation (right).

Experimental

Synthesis of PC-TiO_2-*d*/Cu-TCPP photocatalysts

Synthesis of PC-TiO_2-*d*. In a typical procedure, the solution of 2-aminoterephthalic acid (217 mg, 1.2 mmol) in a mixing solvent of dry DMF (5 mL) and anhydrous methanol (5 mL) was poured into a 25 mL Teflon-lined autoclave including titanium(iv) isopropoxide (0.177 mL, 0.6 mmol). After carefully stirring for 5 min at room temperature, the autoclave was sealed and heated at 150 °C for 15 h in an oven. Afterwards, the mixture was naturally cooled to room temperature, and the yellow powder was collected by centrifugation and washed with DMF and anhydrous ethanol to remove the residual organic ligand and DMF, respectively. Finally, NH_2-MIL-125(Ti) was dried under vacuum at 80 °C for 12 h.

Synthesis of nanosheets assembled porous cages of titanium oxides. The as-formed NH_2-MIL-125(Ti) (10 mg) was uniformly dispersed into a vial containing anhydrous ethanol (5 mL) by sonication. L-alanine (47.5 mg, 0.533 mmol) was introduced to the vial with stirring for 5 min. Subsequently, the vial was placed into to a 25 mL Teflon-lined autoclave and heated at 176 °C for 24 h in an oven. The white precipitate (titanium oxides) was collected by centrifugation, washed with anhydrous ethanol, and dried under vacuum at 80 °C for 12 h.

Synthesis of PC-TiO_2-*d*. The as-made titanium oxide porous cages (30 mg) in a porcelain boat was heated at 590 °C for 30 min through a quartz tube furnace in air. Finally, grey white powder PC-TiO_2-*d* was produced.

Synthesis of 5,10,15,20-tetrakis(4-methoxycarbonylphenyl) porphyrin. Methyl *p*-formylbenzoate (6.9 g, 0.042 mol) was added in a 250 mL round-bottom flask containing propionic acid (100 mL). Pyrrole (3 mL, 0.043 mol) was dropped to the flask. The resultant solution was refluxed for 12 h at 140 °C, and was naturally cooled down to room temperature. The purple precipitate was collected by suction filtration and sequentially washed with methanol, ethyl acetate and THF. The final product was dried in vacuum at 80 °C for 12 h.

Synthesis of [5,10,15,20-tetrakis(4-carboxyphenyl) porphyrine]-Cu (Cu-TCPP). The as-synthesized ester (1.95 g) and $CuCl_2 \cdot 2H_2O$ (2.2 g, 12.8 mmol) dissolved in DMF (100 mL) was refluxed for 6 h. After the mixture was cooled down to room temperature, de-ionized water (150 mL) was added. The red

precipitate was collected by suction filtration, and washed with ethyl acetate and THF in sequence. The final product was dried in vacuum at 80 °C for 12 h. The obtained complex was re-dispersed into a round-bottom flask containing a mixture solvent of THF and methanol (120 mL, V : V = 1 : 1) with stirring. Subsequently, an aqueous solution of KOH (6.28 g, 60 mL) was put into the aforementioned flask. The resultant mixture was refluxed for 12 h at 60 °C and then cooled down to room temperature. Methanol and THF were evaporated from the mixture, and additional de-ionized water was added until the as-formed solid was completely dissolved. Afterwards, the aqueous solution was acidified with HCl (1 M) until no precipitate was further produced. The final purple product (Cu-TCPP) was collected by suction filtration, washed with water and dried in vacuum at 80 °C for 12 h.

Synthesis of PC-TiO_2-*d*/Cu-TCPP. PC-TiO_2-*d* (30 mg) and Cu-TCPP (1.5 mg) were added to a round-bottom flask containing DMF (30 mL). After sonication for 10 min, the flask was kept at room temperature for 12 h with gently stirring. The final product was collected by centrifugation, washed with de-ionized water and ethanol, respectively, and dried in vacuum at 80 °C for 12 h.

Studies of photocatalytic reactions

Photo-degradation of tetracycline. The photocatalytic experiment was carried out in a custom-made reactor (100 mL, Perfectlight, China). The photocatalyst powder (5 mg) was dispersed into an aqueous solution of tetracycline (20 mg L^{-1}, 60 mL). The photocatalytic degradation experiments were performed upon visible light illumination by a 300 W Xe-arc lamp with a UV cutoff filter (λ > 420 nm) or under the simulated sunlight irradiation with an AM 1.5G filter under magnetic stirring gently at room temperature. By tuning the distance between the Xe lamp and the reactor, the luminous power was adjusted to 100 mW cm^{-2}, which was monitored by a power meter (PL-MW2000, Perfectlight, China). Prior to light irradiation, the photo-degradation system was kept at room temperature for 30 min in the dark to fully adsorb tetracycline by photocatalysts.

Photocatalytic coupling reactions between H_2 evolution and tetracycline degradation. The photocatalytic system included photocatalysts (5 mg) and aqueous solutions of tetracycline (20 mg L^{-1}, 60 mL). Prior to light irradiation, the reaction setup was purged by Ar for 30 min to remove all the impurities. The photocatalytic reaction was irradiated with the simulated sunlight under magnetic stirring gently at room temperature. The hydrogen was analysed by using a gas chromatograph (GC7900 Techcomp).

Conclusions

The molecular photosensitizer Cu-TCPP loaded the semiconductor TiO_2 to form the heterogeneous photocatalyst PC-TiO_2-*d*/Cu-TCPP has been successfully prepared by a self-assembly process based on the strong interaction between oxygen vacancies of PC-TiO_2-*d* and Cu(II) ions of metalloporphyrin. The PC-TiO_2-*d*/Cu-TCPP photocatalysts show higher photo-degradation percentage of tetracycline than PC-TiO_2-*d* and TiO_2-*n* under simulated sunlight or visible light irradiation. The high-performance PC-TiO_2-*d*/Cu-TCPP is beneficial from porous structures with high specific surface area, porous structures and strong light harvesting ability of Cu-TCPP in the visible region. In the photo-degradation process, the species of holes, $O_2^{\bullet-}$ and $OH^{\bullet}$ play key roles for tetracycline removal. Finally, the achievement of the coupling of hydrogen evolution and tetracycline degradation without oxygen is due to the presence of holes and $OH^{\bullet}$ radicals. Hence, this research provides a possibility and ideas about preparation of intriguing heterogeneous photocatalysts by combining molecular photosensitizers with semiconductors while achieving the treatment of environmental pharmaceutical pollutants and the acquisition of clean solar fuels.

Author contributions

Conceptualization and methodology: L. Chen and X. Zhang; investigation, visualization, data collection, and validation: H. Lu, X. Wang, G. Li, B. Liao, and J. Tong; formal analysis: X. Zhang, F. Yuan, and Z. Gu; writing – original draft preparation: X. Zhang, L. Chen, and H. Lu; funding acquisition, supervision, writing – review & editing: L. Chen.

Conflicts of interest

There are no conflicts to declare.

Acknowledgements

The authors thank the financial support from Natural Science Foundation of Anhui Province of China (Grant No. 2108085MB47) and Academic Program Foundation of Anhui Province for Top Talents of Universities (Grant No. gxbjZD2022040).

Notes and references

1 T. Ye, H. Liu, W. Qi and J. Qu, Removal of pharmaceutical in a biogenic/chemical manganese oxide system driven by manganese-oxidizing bacteria with humic acids as sole carbon source, *J. Environ. Sci.*, 2023, **26**, 734–741.

2 T. Zhou, Z. Zhang, H. Liu, S. Dong, L. D. Nghiem, L. Gao, A. V. Chaves, A. Zamyadi, X. Li and Q. Wang, A review on microalgae-mediated biotechnology for removing pharmaceutical contaminants in aqueous environments: Occurrence, fate, and removal mechanism, *J. Hazard. Mater.*, 2023, **443**, 130213.

3 M. Patel, R. Kumar, K. Kishor, T. Mlsna, C. U. Pittman, Jr. and D. Mohan, Pharmaceuticals of emerging concern in aquatic systems: chemistry, occurrence, effects, and removal methods, *Chem. Rev.*, 2019, **119**, 3510–3673.

4 B. K. Zaied, M. Rashid, M. Nasrullah, A. W. Zularisam, D. Pant and L. Singh, A comprehensive review on contaminants removal from pharmaceutical wastewater by

electrocoagulation process, *Sci. Total Environ.*, 2020, **726**, 138095.

5 H. Karimi-Maleh, A. Ayati, R. Davoodi, B. Tanhaei, F. Karimi, S. Malekmohammadi, Y. Orooji, L. Fu and M. Sillanpaa, Recent advances in using of chitosan-based adsorbents for removal of pharmaceutical contaminants: A review, *J. Clean. Prod.*, 2021, **291**, 125880.

6 S. Jones, A. Pramanik, R. Kanchanapally, B. P. V. Nellore, S. Begum, C. Sweet and P. C. Rays, Multifunctional three-dimensional chitosan/gold nanoparticle/graphene oxide architecture for separation, label-free SERS identification of pharmaceutical contaminants, and effective killing of superbugs, *ACS Sustainable Chem. Eng.*, 2017, **5**, 7175–7187.

7 M. K. Dail and S. P. Mezyk, Hydroxyl-radical-induced degradative oxidation of beta-lactam antibiotics in water: absolute rate constant measurements, *J. Phys. Chem. A*, 2010, **114**, 8391–8395.

8 P. Liu, H. Zhang, Y. Feng, C. Shen and F. Yang, Integrating electrochemical oxidation into forward osmosis process for removal of trace antibiotics in wastewater, *J. Hazard. Mater.*, 2015, **296**, 248–255.

9 R. Daghrir and P. Drogui, Tetracycline antibiotics in the environment: a review, *Environ. Chem. Lett.*, 2013, **11**, 209–227.

10 J. Oh, C. A. Medriano and S. Kim, The effect of tetracycline in the antibiotic resistance gene transfer before and after ozone disinfection, *Desalin. Water Treat.*, 2016, **57**, 646–650.

11 K. Huang, J. Tang, X.-X. Zhang, K. Xu and H. Ren, A comprehensive insight into tetracycline resistant bacteria and antibiotic resistance genes in activated sludge using next-generation sequencing, *Int. J. Mol. Sci.*, 2014, **15**, 10083–10100.

12 L. Xu, H. Zhang, P. Xiong, Q. Zhu, C. Liao and G. Jiang, Occurrence, fate, and risk assessment of typical tetracycline antibiotics in the aquatic environment: A review, *Sci. Total Environ.*, 2021, **753**, 141975.

13 A. Di Paola, M. Addamo, V. Augugliaro, E. Garcia-Lopez, V. Loddo, G. Marci and L. Palmisano, Photolytic and TiO_2-assisted photodegradation of aqueous solutions of tetracycline, *Fresenius Environ. Bull.*, 2004, **13**, 1275–1280.

14 W. Liu, C. Wei, R. Peng, R. Chu, H. Sun, X. Zhang and F. Xie, Persulfate assisted photocatalytic degradation of tetracycline by bismuth titanate under visible light irradiation, *New J. Chem.*, 2022, **46**, 10854–10862.

15 S. Chavoshan, M. Khodadadi and N. Nasseh, Photocatalytic degradation of penicillin G from simulated wastewater using the UV/ZnO process: isotherm and kinetic study, *J. Environ. Health Sci. Eng.*, 2020, **18**, 107–117.

16 N. Xuan Sang, P. Tien Dung, V. Hoang Tung and N. Kim Dinh, Photocatalytic degradation of cephalexin by g-C_3N_4/Zn doped Fe_3O_4 under visible light, *Environ. Technol.*, 2021, **42**, 1292–1301.

17 W. Deng, H. Zhao, F. Pan, X. Feng, B. Jung, A. Abdel-Wahab, B. Batchelor and Y. Li, Visible-light-driven photocatalytic degradation of organic water pollutants promoted by sulfite addition, *Environ. Sci. Technol.*, 2017, **51**, 13372–13379.

18 F. F. A. Aziz, A. A. Jalil, N. S. Hassan, A. A. Fauzi, M. S. Azami, N. W. C. Jusoh and R. Jusoh, A review on synergistic coexisting pollutants for efficient photocatalytic reaction in wastewater remediation, *Environ. Res.*, 2022, **209**, 112748.

19 T. S. Natarajan, K. R. Thampi and R. J. Tayade, Visible light driven redox-mediator-free dual semiconductor photocatalytic systems for pollutant degradation and the ambiguity in applying Z-scheme concept, *Appl. Catal., B*, 2018, **227**, 296–311.

20 D. S. Achilleos, H. Kasap and E. Reisner, Photocatalytic hydrogen generation coupled to pollutant utilisation using carbon dots produced from biomass, *Green Chem.*, 2020, **22**, 2831–2839.

21 C. Long, X. Dong and J. Huang, Latest progress on photocatalytic H_2 production by water splitting and H_2 production coupled with selective oxidation of organics over $ZnIn_2S_4$-based photocatalysts, *Energy Fuels*, 2022, **37**, 136–158.

22 M. I. Badawy, M. Y. Ghaly and M. E. M. Ali, Photocatalytic hydrogen production over nanostructured mesoporous titania from olive mill wastewater, *Desalination*, 2011, **267**, 250–255.

23 J. Kim, D. Monllor-Satoca and W. Choi, Simultaneous production of hydrogen with the degradation of organic pollutants using TiO2 photocatalyst modified with dual surface components, *Energy Environ. Sci.*, 2012, **5**, 7647.

24 J. Schneider, M. Matsuoka, M. Takeuchi, J. Zhang, Y. Horiuchi, M. Anpo and D. W. Bahnemann, Understanding TiO_2 photocatalysis: Mechanisms and materials, *Chem. Rev.*, 2014, **114**, 9919–9986.

25 M. Nolan, A. Iwaszuk, A. K. Lucid, J. J. Carey and M. Fronzi, Design of novel visible light active photocatalyst materials: surface modified TiO_2, *Adv. Mater.*, 2016, **28**, 5425–5446.

26 K. E. Dalle, J. Warnan, J. J. Leung, B. Reuillard, I. S. Karmel and E. Reisner, Electro- and solar-driven fuel synthesis with first row transition metal complexes, *Chem. Rev.*, 2019, **119**, 2752–2875.

27 T. Morikawa, S. Sato, K. Sekizawa, T. M. Suzuki and T. Arai, Solar-driven CO_2 reduction using a semiconductor/molecule hybrid photosystem: from photocatalysts to a monolithic artificial leaf, *Acc. Chem. Res.*, 2022, **55**, 933–943.

28 Z. Huang and M. L. Tang, Designing transmitter ligands that mediate energy transfer between semiconductor nanocrystals and molecules, *J. Am. Chem. Soc.*, 2017, **139**, 9412–9418.

29 S. Hiroto, Y. Miyake and H. Shinokubo, Synthesis and functionalization of porphyrins through organometallic methodologies, *Chem. Rev.*, 2017, **117**, 2910–3043.

30 S. Kundu and A. Patra, Nanoscale strategies for light harvesting, *Chem. Rev.*, 2017, **117**, 712–757.

31 K. Zeng, Z. Tong, L. Ma, W.-H. Zhu, W. Wu and Y. Xie, Molecular engineering strategies for fabricating efficient porphyrin-based dye-sensitized solar cells, *Energy Environ. Sci.*, 2020, **13**, 1617–1657.

32 W. Zhou, W. Li, J. Q. Wang, Y. Qu, Y. Yang, Y. Xie, K. Zhang, L. Wang, H. Fu and D. Zhao, Ordered mesoporous black

TiO_2 as highly efficient hydrogen evolution photocatalyst, *J. Am. Chem. Soc.*, 2014, **136**, 9280–9283.

33 B. Sun, W. Zhou, H. Li, L. Ren, P. Qiao, W. Li and H. Fu, Synthesis of particulate hierarchical tandem heterojunctions toward optimized photocatalytic hydrogen production, *Adv. Mater.*, 2018, **30**, e1804282.

34 Z. Li, H. Li, S. Wang, F. Yang and W. Zhou, Mesoporous black $TiO_2/MoS_2/Cu_2S$ hierarchical tandem heterojunctions toward optimized photothermal-photocatalytic fuel production, *Chem. Eng. J.*, 2022, **427**, 131830.

35 Z. Xiu, M. Guo, T. Zhao, K. Pan, Z. Xing, Z. Li and W. Zhou, Recent advances in Ti^{3+} self-doped nanostructured TiO2 visible light photocatalysts for environmental and energy applications, *Chem. Eng. J.*, 2020, **382**, 123011.

36 Z. Li, S. Wang, J. Wu and W. Zhou, Recent progress in defective TiO_2 photocatalysts for energy and environmental applications, *Renewable Sustainable Energy Rev.*, 2022, **156**, 111980.

37 J. Wan, W. Chen, C. Jia, L. Zheng, J. Dong, X. Zheng, Y. Wang, W. Yan, C. Chen, Q. Peng, D. Wang and Y. Li, Defect effects on TiO_2 nanosheets: stabilizing single atomic site au and promoting catalytic properties, *Adv. Mater.*, 2018, **30**, 1705369.

38 Z. Gu, L. Chen, X. Li, L. Chen, Y. Zhang and C. Duan, NH_2-MIL-125(Ti)-derived porous cages of titanium oxides to support Pt-Co alloys for chemoselective hydrogenation reactions, *Chem. Sci.*, 2019, **10**, 2111–2117.

39 J. Tong, J. Wang, X. Shen, H. Zhang, Y. Wang, Q. Fang and L. Chen, One-pot synthesis of schiff bases by defect-induced TiO_{2-x}-catalyzed tandem transformation from alcohols and nitro compounds, *Inorg. Chem.*, 2021, **60**, 10715–10721.

40 F. Lei, Y. Sun, K. Liu, S. Gao, L. Liang, B. Pan and Y. Xie, Oxygen vacancies confined in ultrathin indium oxide porous sheets for promoted visible-light water splitting, *J. Am. Chem. Soc.*, 2014, **136**, 6826–6829.

41 Q. Zhu, Y. Peng, L. Lin, C.-M. Fan, G.-Q. Gao, R.-X. Wang and A.-W. Xu, Stable blue TiO_{2-x} nanoparticles for efficient visible light photocatalysts, *J. Mater. Chem. A*, 2014, **2**, 4429.

42 D. Feng, Z. Y. Gu, J. R. Li, H. L. Jiang, Z. Wei and H. C. Zhou, Zirconium-metalloporphyrin PCN-222: mesoporous metal-organic frameworks with ultrahigh stability as biomimetic catalysts, *Angew. Chem., Int. Ed.*, 2012, **51**, 10307–10310.

43 W. Lian, Y. Sun, B. Wang, N. Shan and T. Shi, Synthesis and properties of 5,10,15,20-tetra[4-(3,5-dioctoxybenzamidephenyl)] porphyrin and its metal complexes, *J. Serb. Chem. Soc.*, 2012, **77**, 335–348.

44 R. N. Mozhchil, A. M. Ionov, S. I. Bozhko, V. S. Bozhko, V. D. Rumyantseva, A. L. Trigub and A. P. Menushenkov, Electronic, local atomic structure of lutetium tetraphenylporfyrin: XPS and XAFS spectroscopy stadies, *J. Phys.: Conf. Ser.*, 2019, **1238**, 012002.

45 S. Jin, H. J. Son, O. K. Farha, G. P. Wiederrecht and J. T. Hupp, Energy transfer from quantum dots to metal-organic frameworks for enhanced light harvesting, *J. Am. Chem. Soc.*, 2013, **135**, 955–958.

46 B. B. Beyene and C.-H. Hung, Porphyrin-based electrochemical H_2 evolution: role of central metal ion on overpotential and catalytic activity, *Electrocatalysis*, 2018, **9**, 689–696.

47 L. F. Schneemeyer and M. S. Wrighton, Flat-band potential of n-type semiconducting molybdenum disulfide by cyclic voltammetry of two-electron reductants: interface energetics and the sustained photooxidation of chloride, *J. Am. Chem. Soc.*, 1979, **101**, 6496–6500.

48 J. Shang, W. Hao, X. Lv, T. Wang, X. Wang, Y. Du, S. Dou, T. Xie, D. Wang and J. Wang, Bismuth oxybromide with reasonable photocatalytic reduction activity under visible light, *ACS Catal.*, 2014, **4**, 954–961.

49 Y. Xu and M. A. A. Schoonen, The absolute energy positions of conduction and valence bands of selected semiconducting minerals, *Am. Mineral.*, 2000, **85**, 543–556.

50 C. Wang, M. Cai, Y. Liu, F. Yang, H. Zhang, J. Liu and S. Li, Facile construction of novel organic-inorganic tetra (4-carboxyphenyl) porphyrin/Bi(2)MoO(6) heterojunction for tetracycline degradation: Performance, degradation pathways, intermediate toxicity analysis and mechanism insight, *J. Colloid Interface Sci.*, 2022, **605**, 727–740.

51 S. Xing, T. Li, Y. Gao and J. Liu, Insight into the mechanism for photocatalytic degradation of ciprofloxacin with CeO_2, *Optik*, 2019, **183**, 266–272.